Biochemical Pharmacology 92 (2014) 690–700

Contents lists available at ScienceDirect

Biochemical Pharmacology

journal homepage: www.elsevier.com/locate/biochempharm

Identification of CYP3A7 for glyburide metabolism in human fetal livers

Diana L. Shuster [a], Linda J. Risler [b], Bhagwat Prasad [a], Justina C. Calamia [a], Jenna L. Voellinger [a], Edward J. Kelly [a], Jashvant D. Unadkat [a], Mary F. Hebert [b,c], Danny D. Shen [a,b], Kenneth E. Thummel [a], Qingcheng Mao [a,*]

[a] Department of Pharmaceutics, School of Pharmacy, University of Washington, Box 357610, Seattle, WA 98195, USA
[b] Department of Pharmacy, University of Washington, Box 357630, Seattle, Washington 98195, USA
[c] Department of Obstetrics and Gynecology, University of Washington, Box 356460, Seattle, Washington 98195, USA

ARTICLE INFO

Article history:
Received 29 August 2014
Received in revised form 2 September 2014
Accepted 29 September 2014
Available online 22 October 2014

Chemical compounds studied in this article:
Glyburide (PubChem CID: 3488)
Dehydroepiandrosterone (PubChem CID: 5881)
16α-hydroxydehydroepiandrosterone (PubChem CID: 102030)
Midazolam (PubChem CID: 4192)
1′-Hydroxymidazolam (PubChem CID: 107917)
4′-Hydroxymidazolam (Pubchem CID: 124449)

Keywords:
CYP3A7
Fetal metabolism
Glyburide
Human fetal livers
Gestational diabetes mellitus

ABSTRACT

Glyburide is commonly prescribed for the treatment of gestational diabetes mellitus; however, fetal exposure to glyburide is not well understood and may have short- and long-term consequences for the health of the child. Glyburide can cross the placenta; fetal concentrations at term are nearly comparable to maternal levels. Whether or not glyburide is metabolized in the fetus and by what mechanisms has yet to be determined. In this study, we determined the kinetic parameters for glyburide depletion by CYP3A isoenzymes; characterized glyburide metabolism by human fetal liver tissues collected during the first or early second trimester of pregnancy; and identified the major enzyme responsible for glyburide metabolism in human fetal livers. CYP3A4 had the highest metabolic capacity towards glyburide, followed by CYP3A7 and CYP3A5 ($Cl_{int,u}$ = 37.1, 13.0, and 8.7 ml/min/nmol P450, respectively). M5 was the predominant metabolite generated by CYP3A7 and human fetal liver microsomes (HFLMs) with approximately 96% relative abundance. M5 was also the dominant metabolite generated by CYP3A4, CYP3A5, and adult liver microsomes; however, M1–M4 were also present, with up to 15% relative abundance. CYP3A7 protein levels in HFLMs were highly correlated with glyburide Cl_{int}, 16α-OH DHEA formation, and 4′-OH midazolam formation. Likewise, glyburide Cl_{int} was highly correlated with 16α-OH DHEA formation. Fetal demographics as well as CYP3A5 and CYP3A7 genotype did not alter CYP3A7 protein levels or glyburide Cl_{int}. These results indicate that human fetal livers metabolize glyburide predominantly to M5 and that CYP3A7 is the major enzyme responsible for glyburide metabolism in human fetal livers.

1. Introduction

During pregnancy, 5–14% of women will be diagnosed with gestational diabetes mellitus (GDM) [1,2]. Glyburide is an oral hypoglycemic drug that is prescribed more commonly for the treatment of GDM than before [3]. Though glyburide exhibits nearly comparable efficacy to insulin, the incidence rates of adverse fetal effects associated with glyburide verses insulin therapy, such as neonatal hypoglycemia and large for gestational age infants, are conflicting [4–8]. At present, there are no long-term safety data for infants whose mothers were treated with glyburide. In addition, studies are needed to understand the mechanistic determinants of fetal exposure that impact the fetal safety of glyburide.

Glyburide is extensively metabolized in the maternal liver by CYP3A4, CYP2C9, and CYP2C19 to several metabolites, such as 4-*trans*-hydroxycyclohexyl glyburide (M1), 4-*cis*-hydroxycyclohexyl glyburide (M2a), 3-*cis*-hydroxycyclohexyl glyburide (M2b),

* Corresponding author. Department of Pharmaceutics, University of Washington, Box 357610, Seattle, WA 98195, USA. Tel.: +1 206 685 0355; fax: +1 206 543 3204.
E-mail addresses: dshust@uw.edu (D.L. Shuster), lrisler@uw.edu (L.J. Risler), bhagwat@uw.edu (B. Prasad), jcalamia@uw.edu (J.C. Calamia), jennav2@uw.edu (J.L. Voellinger), edkelly@uw.edu (E.J. Kelly), jash@uw.edu (J.D. Unadkat), mhebert@uw.edu (M.F. Hebert), ds@uw.edu (D.D. Shen), thummel@uw.edu (K.E. Thummel), qmao@uw.edu (Q. Mao).

http://dx.doi.org/10.1016/j.bcp.2014.09.025
0006-2952/

3-*trans*-hydroxycyclohexyl glyburide (M3), 2-*trans*-hydroxycyclohexyl glyburide (M4), and ethylene-hydroxylated glyburide (M5); though there may be more [9,10]. As treatment of GDM with glyburide is optimized, there will be several factors that could be important determinants of fetal exposure to glyburide and its metabolites, (and ultimately its safety profile), including maternal exposure, transplacental clearance, placental metabolism, and fetal elimination. Maternal exposure to conventional doses of glyburide during human pregnancy is reduced compared to non-pregnant women, suggesting the need for increased doses [11]. Glyburide concentrations, which are measurable in umbilical cord blood at the time of delivery, suggest that glyburide can cross the placenta [11]. ATP-binding cassette (ABC) efflux transporters, particularly breast cancer resistance protein (BCRP) and P-glycoprotein (P-gp) are highly expressed in the placenta and may limit fetal glyburide exposure to some extent [12–18]. Since the expression of ABC transporters in the placenta changes as gestation progresses [15] and the placenta grows larger with gestational age, penetration of glyburide into the fetal compartment across the placental barrier may also change over gestation. In addition, glyburide can be metabolized in human term placenta [9,10,19,20], specifically by the cytochrome P450 (CYP) enzyme CYP19 (aromatase). Although the relative contribution of placental drug-metabolizing enzymes to the overall maternal disposition of glyburide may in fact be minimal, glyburide metabolism in such close proximity to the fetus could possibly affect fetal exposure to glyburide and its metabolites. Metabolite transplacental clearances have not been determined, however. Finally, fetal exposure to glyburide may also be influenced by fetal liver metabolism upon entrance into the fetal circulation. At present, little is known about glyburide metabolism in human fetal livers.

CYP3A7 is the predominant CYP enzyme in the human fetal liver [21–23]. CYP3A5 has also been found in the human fetal liver [24], but at much lower amounts relative to CYP3A7. In a panel of human fetal livers ($n \sim 10$), the mRNA levels of CYP3A5 were approximately 700-fold lower than those of CYP3A7, and CYP3A5 protein was detected in just one liver (CYP3A5 genotype was not determined) [23]. Previous studies using adult human liver microsomes (HLMs) and recombinant enzymes have shown that glyburide is a substrate of CYP3A4 and CYP3A5 [9,25], suggesting the plausibility of glyburide metabolism by other CYP3A isoforms such as CYP3A7. Indeed, CYP3A7 has been shown to metabolize endogenous substrates of CYP3A4, such as testosterone and dehydroepiandrosterone (DHEA), but with different oxidation site preferences [22,26]. Several *in vitro* studies have also shown that both embryonic (less than 60 days) and fetal livers can metabolize endogenous compounds (i.e. testosterone, retinoic acid, and DHEA) and xenobiotics (i.e. warfarin, benzyloxyresorufin, and coumarin), as well as activate promutagens and procarcinogens [27,28]. CYP3A7 preferentially metabolizes testosterone to its 2α–OH metabolite, rather than its 6β–OH metabolite, which is primarily produced by CYP3A4 [22], suggesting the metabolic profile of glyburide in human fetal livers could differ from that in adult livers. Given that glyburide can cross the placental barrier [11,29] and that CYP3A7 expression/activity is variable in human fetal livers [22], it is important to investigate CYP3A7-mediated metabolism of glyburide and characterize the variability of glyburide metabolism in human fetal livers. Understanding fetal metabolism of glyburide is clinically relevant because this may govern fetal exposure to not only glyburide, but its major metabolites such as M1 and M2b, which are believed to be pharmacologically active [30].

In this study, we determined the kinetics of glyburide depletion by CYP3A4, CYP3A5, and CYP3A7 supersomes, measured the Cl_{int} of glyburide in human fetal liver microsomes (HFLMs), and compared the metabolite profiles generated by CYP3A supersomes, HFLMs, and HLMs. We examined the correlation between glyburide Cl_{int} and metabolism of DHEA (a known CYP3A7 probe substrate) as well as midazolam (a CYP3A substrate) in human fetal livers. To better understand sources of variability in fetal metabolism, we also investigated the relationship between glyburide Cl_{int} and CYP3A7 protein levels in human fetal livers, fetal liver gestational age, fetal sex, CYP3A7 genotype, and other fetal demographics. Results from this study will have important clinical implications for informing fetal exposure and the fetal safety profile of glyburide in early and mid-gestation.

2. Materials and methods

2.1. Materials

Glyburide and glipizide (internal standard) were purchased from Sigma–Aldrich (St. Louis, MO). The following glyburide metabolites were purchased from TLC PharmaChem (Vaughan, Ontario, Canada): 4-*trans*-hydroxycyclohexyl glyburide (M1), 3-*cis*-hydroxycyclohexyl glyburide (M2b), and 3-*trans*-hydroxycyclohexyl glyburide (M3). 4-*cis*-hydroxycyclohexyl glyburide (M2a) was a generous gift from the University of Texas Medical Branch in Galveston. [Cyclohexyl-2,3-^{3}H(N)]-glyburide ([^{3}H]-Gly) (50 Ci/mmol) was obtained from PerkinElmer Life and Analytical Sciences (Waltham, MA). Midazolam (MDZ) was purchased from Sigma–Aldrich (St. Louis, MO). 1′-OH Midazolam (1′-OH MDZ) and 4′-OH Midazolam (4′-OH MDZ) were purchased from Ultrafine (Manchester, England). Internal standards for the metabolites of MDZ, $^{15}N_3$-1′-OH MDZ and $^{15}N_3$-4′-OH MDZ, were prepared as previously described [31]. Dehydroepiandrosterone (DHEA) and its metabolite, 16α-hydroxydehydroepiandrosterone (16α-OH DHEA) were purchased from Steraloids (Newport, RI). Iodoacetamide, dithiothreitol and sequencing grade trypsin were purchased from Pierce Biotechnology (Rockford, IL). Ammonium bicarbonate was purchased from Acros Organics (Geel, Belgium). Sodium deoxycholate was purchased from MP Biologicals (Santa Ana, California). Synthetic light peptides for CYP enzyme quantification were procured from New England Peptides (Boston, MA), with purity established by amino acid analysis. Heavy stable isotope labeled amino acids, [$^{13}C_6{}^{15}N_2$]-lysine and [$^{13}C_6{}^{15}N_4$]-arginine, were purchased from Pierce Biotechnology, Inc. (Rockford, IL). β-Nicotinamide adenine dinucleotide 2′-phosphate reduced (NADPH) tetrasodium salt hydrate, potassium phosphate monobasic and dibasic, ethylenediaminetetraacetic acid (EDTA), and HPLC-grade formic acid were purchased from Sigma-Aldrich (St. Louis, MO). Potassium phosphate dibasic, ethyl acetate, and HPLC-grade methanol, acetonitrile, and ammonium formate were obtained from Thermo Fisher Scientific (Waltham, MA). CYP3A4, CYP3A5 and CYP3A7 Supersomes™ were purchased from BD Biosciences (San Jose, California). Pooled HLMs were purchased from Xenotech (Lenexa, KS).

2.2. Preparation of human fetal liver microsomes (HFLMs)

Sixteen human fetal livers from first and second trimester pregnancies were obtained from the University of Washington Birth Defects Research Laboratory. HFLMs were prepared as described previously [32,33]. Briefly, approximately 1 g of fetal liver tissue was homogenized in 3 ml of homogenization buffer (50 mM KPi buffer containing 0.25 M sucrose and 1 mM EDTA, pH 7.4) using an Omni Bead Ruptor Homogenizer (Omni International, Kennesaw, GA). The homogenate was centrifuged at 15,000 × *g* for 30 min at 4 °C, and the supernatant at 120,000 × g for 70 min at 4 °C. Microsomal pellets were resuspended in 1 ml storage buffer (50 mM KPi buffer, 0.25 M sucrose, and 10 mM EDTA, pH 7.4), and stored at −80 °C until use. Microsomal protein concentrations were determined using the Pierce BCA Protein Assay Kit (Thermo

Scientific, Rockford, IL) with bovine serum albumin as the standard.

2.3. DNA isolation and CYP3A genotyping of human fetal livers

DNA was isolated from 16 human fetal liver samples using a Qiagen (Valencia, California) DNeasy Blood and Tissue Kit according to the manufacturer's recommendations. For allele nomenclature, the CYPallele Nomenclature Guidelines (http://www.imm.ki.se/cypalleles) were used with *CYP3A5*1* and *CYP3A7*1* as reference sequences. Genotyping for alleles *CYP3A5*3* (C__26201809_30) and **6* (C__30203950_10) as well as *CYP3A7*2* (C__25474551_10) and **1C* (T > A: C__30634321_20; G > T: C__30634326_10) was performed using pre-developed TaqMan assays purchased from Invitrogen (Grand Island, NY).

2.4. Quantification of CYP protein in human fetal liver microsomes by HPLC-MS/MS

Simultaneous quantification of multiple CYP enzymes was carried out using a surrogate peptide-based HPLC-MS/MS method. The surrogate light peptides were first selected based on previously reported criteria [34,35]. The corresponding heavy peptides containing labeled [$^{13}C_6{}^{15}N_2$]-lysine or [$^{13}C_6{}^{15}N_4$]-arginine residues were used as internal standards. Prior to CYP quantification, fetal liver microsomal samples were diluted to 2 mg/ml, and 20 μl (40 μg of protein) was subsequently digested using a previously validated protocol with a few modifications [36]. Briefly, microsomal samples were denatured and reduced via incubation with 4 μl of 100 mM dithiothreitol, 10 μl of sodium deoxycholate (2.6% w/v) and 10 μl of ammonium bicarbonate buffer (100 mM) at 95 °C for 5 min. The protein samples were then cooled and alkylated using 4 μl of 200 mM iodoacetamide at room temperature in the dark. The samples were digested with 10 μl of trypsin in a final volume of 48 μl at 37 °C for 22 h. The reaction was stopped by the addition of 20 μl of peptide internal standard cocktail (prepared in 50% acetonitrile in water containing 0.1% formic acid) and 10 μl of the neat solvent, i.e., 50% acetonitrile in water containing 0.1% formic acid. The samples were vortexed and centrifuged at 3500 × *g* for 5 min. Calibration curve standards were prepared by spiking standard working solutions of peptides into a solution containing all of the above mentioned reagents plus microsomal storage buffer (Section 2.2) to replace microsomal sample. Eight calibration concentrations ranging from approximately 0.3 to 600 fmol peptide (on column) were used for various CYP enzymes. For each standard, working stock solutions of the peptide (10 μl) were added in the last step instead of the neat solvent. The supernatant was transferred to HPLC vials and stored at −20 °C until further analysis by HPLC-MS/MS. Digestion and quantification were performed in triplicate for each HFLM sample. Two pooled (n = 10) HLM samples from adult donors were also processed similarly to serve as quality controls for the HPLC-MS/MS method.

The CYP protein quantification assays were performed on a triple-quadrupole LC-MS instrument (Agilent 6460A) coupled to an Agilent 1290 Infinity LC system (Agilent Technologies), in ESI positive ionization mode. Approximately 2 μg of the trypsin digest (5 μl) was injected onto the column (Kinetex 1.7 μ, C18 100A; 100 × 2.1 mm, Phenomenex, Torrance, CA). Mobile phases consisted of water (A) and acetonitrile (B) (both containing 0.1% formic acid) at a flow rate of 0.3 ml/min. The gradient was 3% mobile phase B for 2.0 min, followed by gradient elution program with mobile phase B concentration of 3 to 18% (2.0–4.0 min), 18 to 22% (4.0–8.0 min), 22 to 24% (8.0–10 min), 24% (10–12.2 min), 24 to 34% (12.2–12.5 min) and 34 to 38% (12.5–15.0 min). This was followed by washing with 80% mobile phase B for 0.9 min and re-equilibration for 4.9 min. Surrogate peptides and internal standards were monitored in multiple reaction monitoring (MRM) mode using instrument parameters provided in Table 1. HPLC-MS/MS data were

Table 1
Optimized MS/MS parameters used for quantification of surrogate peptides and internal standards of CYP enzymes in trypsin digested microsomes.

Enzyme	Peptide	Precursor ion (m/z)	Product ion (m/z)	Fragmentor (V)	Collision energy (eV)	LLOQ (fmol on-column)
CYP3A4	LSLGGLLQPEKPVVLK	564.6	746	100	9	0.3
		564.6	689.4	100	10	
	LSLGGLLQPEKPVVLK	567.3	750	100	9	
		567.3	693.4	100	9	
CYP3A5	DSIDPYIYTPFGTGPR	900.0	995.7	130	28	1
		900.0	684.9	130	20	
	DSIDPYIYTPFGTGPR	904.9	1005.5	130	28	
		904.9	689.9	130	28	
CYP3A7	FNPLDPFVLSIK	695.4	918.4	110	16	0.1
		695.4	564.7	110	16	
	FNPLDPFVLSIK	699.4	926.5	110	16	
		699.4	568.8	110	16	
CYP2C9	GIFPLAER	451.9	585.4	75	7	0.15
		451.9	366.8	75	7	
	GIFPLAER	456.8	595.3	75	7	
		456.8	371.7	75	7	
CYP2C19	IYGPVFTLYFGLER	838.0	1145.4	145	28	1
		838.0	998.3	145	28	
	IYGPVFTLYFGLER	843.0	1155.6	145	28	
		843.0	1008.5	145	28	
CYP2A6	GTGGANIDPTFFLSR	777.1	982.5	130	22	0.4
		777.1	867.2	130	26	
	GTGGANIDPTFFLSR	781.9	992.5	130	26	
		781.9	877.5	130	26	
CYP2D6	GTTLITNLSSVLK	673.9	974.4	110	16	0.6
		673.9	861.3	110	16	
	GTTLITNLSSVLK	677.9	982.4	110	16	
		677.9	869.3	110	16	
CYP reductase	FAVFGLGNK	476.9	734.3	100	9	0.05
		476.9	635.3	100	9	
	FAVFGLGNK	480.8	742.4	100	9	
		480.8	643.4	100	9	

Underlined residues represent the internal standards with the labeled [$^{13}C_6{}^{15}N_2$]-lysine or [$^{13}C_6{}^{15}N_4$]-arginine.

processed using the MassHunter (Agilent Technologies) and Skyline software.

2.5. Glyburide depletion kinetics in CYP3A supersomes and HFLMs, and quantification by HPLC-MS

Incubations and reaction conditions were adapted from published methods [22,25]. Briefly, supersome reaction mixtures contained varying glyburide concentrations (0.01–20 μM) dissolved in methanol (<1% v/v), CYP3A4, CYP3A5, or CYP3A7 supersomes, and 100 mM potassium phosphate buffer (1 mM EDTA, pH 7.4), in a final volume of 200 μl. The concentrations of CYP3A4, CYP3A5 or CYP3A7 supersomes in reaction mixtures were 10, 30, and 50 pmol/ml, respectively. HFLM reaction mixtures were prepared similarly, except that only one concentration of glyburide was used (0.05 μM) with 0.8 mg/ml of microsomal protein. After pre-incubation in a shaking 37 °C water bath for 5 min, reactions were initiated by adding NADPH to a final concentration of 1 mM. Supersome reactions were stopped at 0, 5, 10, 15, 20, 30, and 45 min; HFLM reactions were stopped at 0, 15, 30, and 45 min, both with 200 μl of ice-cold methanol (for glyburide concentrations ≤ 0.5 μM) or 1 ml of ice-cold methanol (for glyburide concentrations > 0.5 μM). Incubations without NADPH at 0 and 45 min served as negative controls. No depletion was observed in the absence of NADPH. Following the addition of 20 μl of glipizide (internal standard, 1 ng/μl in methanol), samples were briefly vortexed and centrifuged at 20,800 × *g* for 10 min at 4 °C. The supernatant was transferred to a 96-well plate and 1 μl was injected for analysis by HPLC-MS. To determine CYP3A supersome kinetics, three experiments were performed for each CYP3A isoform. In a given experiment, triplicate determinations were performed for each time point. To determine the intrinsic clearance (Cl_{int}) of glyburide in individual HFLMs, one experiment was performed using duplicate determinations for each time point. Due to the limited amount of fetal liver microsomal protein, only one depletion experiment was performed for each HFLM. Glyburide concentrations were quantified using a validated HPLC-MS assay as previously described [37]. Two calibration curves (low and high) were prepared using potassium phosphate buffer as a matrix over the concentration ranges of 2.5–500 ng/ml (5 nM–1 μM) and 25–10,000 ng/ml (0.05–20 μM) glyburide.

Glyburide concentrations remaining at various time points were analyzed graphically on a semilogarithmic plot. The first-order rate constant for glyburide depletion (k_{dep}, min^{-1}) was estimated by least-squares regression of the entire depletion curve using the Graphpad Prism 6.04 software (La Jolla, CA). For CYP3A supersome kinetics, depletion rates were converted to reaction velocities (v) using the following equation:

$$v = (k_{dep} \cdot [S_0])/[\text{rCYP}]$$

where $[S_0]$ is the initial glyburide concentration (ranging from 0.01–20 μM) and [rCYP] is the concentration of the recombinant enzyme used in the incubation. Reaction velocities were plotted against initial glyburide concentrations ($[S_0]$), and kinetic parameters (K_m and V_{max}) were estimated from a least-squares regression fit to a Michaelis-Menten equation using the Graphpad Prism 6.04 software [38]. As mentioned previously, three separate experimental determinations were completed to estimate kinetic parameters for each of the CYP3A isoforms. Statistically significant differences between mean parameter estimates of different CYP3A isoforms were determined using one-way ANOVA analysis followed by the Tukey's multiple comparison test (n = 3 per CYP3A isoform).

For individual HFLM's, the Cl_{int} was calculated as previously described using the following equation [37,38]:

$$Cl_{int} = k_{dep}/\text{microsomal protein concentration}$$

Linear correlations between glyburide Cl_{int}, CYP3A7 protein levels, 16α-OH DHEA formation, 1′-OH MDZ formation and 4′-OH MDZ formation were evaluated by estimating the Pearson correlation coefficient (r) using the Graphpad Prism 6.04 software.

2.6. Metabolite profile of glyburide in CYP3A supersomes, HFLMs, and HLMs and relative abundance by HPLC-MS/MS

The metabolite profile of glyburide was determined with CYP3A4, CYP3A5 and CYP3A7 supersomes as well as pooled HFLMs and pooled HLMs. Reaction mixtures contained 0.05 μM glyburide dissolved in methanol (<1% v/v), 30 pmol/ml CYP3A supersomes or 0.8 mg/ml microsomal protein, and 100 mM potassium phosphate (KH_2PO_4) buffer (1 mM EDTA, pH 7.4), in a final volume of 200 μl. Incubations were performed according to section 2.5, except for two minor modifications: reactions were stopped at 30 min rather than 45 min, and 5 μl of supernatant were injected for HPLC-MS/MS analysis. One experiment was performed using duplicate determinations for each time point.

Metabolites M1-M5 were identified by HPLC-MS/MS using an Agilent series 1200 HPLC interfaced with an Agilent 6410 triple quadrupole mass spectrometer (Agilent Technologies, Palo Alto, CA). Separation of M1-M5, glyburide, and glipizide was achieved using an ACE C8 300 column (150 mm × 2.1 mm × 3 μ) with gradient elution. The mobile phases consisted of methanol (B) and 5 mM ammonium formate (pH 6) (A). The flow rate was set to 0.4 ml/min. The gradient was 40% methanol for the first 5 min, increased linearly to 90% for 4 min, held for 2 min at 90% methanol, and immediately decreased to 40%, and held at 40% for the remainder of the 15 min run time. The mass spectrometer was run in ESI positive ionization mode with a capillary voltage of 3500 V and a fragmentation voltage of 110 V for all metabolites and 87 V for glipizide. The drying gas temperature was 350 °C, the nitrogen drying gas flow rate was 10.0 L/min, and the nebulizer pressure was 35 pound-force per square-inch-gauge. Since a standard for M5 is not commercially available, metabolite identification was based on elution order and ion transitions as previously described [39]. The following ion transitions were monitored in MRM mode: m/z 510.2 > 169.0, 367.0, and 369.0 for M1–M5, m/z 494.2 > 169.0 for glyburide, and m/z 446.2 > 321.1 for glipizide. HPLC-MS/MS data were processed using MassHunter (Agilent Technologies). Peak area ratios were used to compare relative abundance of metabolites between CYP3A supersomes, HFLMs, and HLMs, assuming that fragment ion signal to on-column injected molar amount is about the same for all the analytes.

2.7. 16α-OH-DHEA formation in HFLMs and quantification by HPLC-MS

16α-OH-DHEA formation in HFLMs was performed as previously described with minor modifications [22]. Briefly, reaction mixtures contained 100 μM DHEA (dissolved in 100% v/v methanol, dried down under air, and reconstituted in HFLM protein/buffer mixture), 0.8 mg/ml HFLMs, and 100 mM potassium phosphate buffer (1 mM EDTA, pH 7.4), in a final volume of 100 μl. After pre-incubating in a shaking 37 °C water bath for 5 min, reactions were initiated by adding NAPDH to a final concentration of 1 mM. Reactions were stopped at 0 and 10 min with 1 ml of ice-cold methanol. Incubations using HFLMs without NADPH at 0 and 10 min served as negative controls. Following the addition of 20 μl

of progesterone (internal standard, 5.0 μg/ml in methanol), samples were briefly vortexed and centrifuged at 20,800 × *g* for 10 min at 4 °C. The supernatant was transferred to a 96-well plate and 1 μl was injected for analysis by HPLC-MS. Due to the limited amount of fetal liver microsomal protein, only one depletion experiment was performed for each HFLM; however, duplicate determinations were performed for each time point. Under these conditions, the depletion of DHEA did not exceed 20%.

DHEA and 16α-OH-DHEA concentrations were quantified by HPLC-MS using an Agilent series 1100 HPLC interfaced with an Agilent G1956B single quadrupole mass spectrometer (Agilent Technologies, Palo Alto, CA). Separation of DHEA and 16α-OH-DHEA was achieved using a Zorbax C18 extend column (50 mm × 2.1 mm × 5 μ) with gradient elution. The mobile phases consisted of methanol (B) and water containing 0.1% formic acid (A). The flow rate was set to 0.3 ml/min. The gradient was 40% methanol for the first 3 min, increased linearly to 80% for 7 min, and held for 2 min at 80% methanol for the remainder of the 12 min run time. The mass spectrometer was run in API-ES positive ionization mode with a capillary voltage of 3750 V and a fragmentation voltage of 70 V for DHEA and 100 V for 16α-OH-DHEA and progesterone. The drying gas temperature was 350 °C, the nitrogen drying gas flow rate was 10.0 L/min, and the nebulizer pressure was 35 pound-force per square-inch-gauge. Ions monitored were 271 *m/z* for DHEA, 315 *m/z* for progesterone, and 322 *m/z* for 16α-OH-DHEA. A calibration curve was prepared using potassium phosphate buffer as a matrix over the concentration range of 500–20,000 ng/ml (1.6–65 μM) DHEA. The lower limit of quantification in potassium phosphate buffer was 473.5 ng/ml with an accuracy of 103% and a precision of 11.4%.

2.8. 1′-OH MDZ and 4′-OH MDZ formation in HFLMs and quantification by HPLC-MS/MS

1′-OH MDZ and 4′-OH MDZ formation in HFLMs was performed as previously described with minor modifications [31]. Briefly, reaction mixtures contained 8 μM midazolam dissolved in <1% (v/v) methanol, 0.1 mg/ml HFLMs, and 100 mM potassium phosphate (KH_2PO_4) buffer (3 mM $MgCl_2$, 1 mM EDTA, pH 7.4), in a final volume of 250 μl. After pre-incubating in a shaking 37 °C water bath for 5 min, reactions were initiated with 1 mM NADPH. Reactions were stopped at 0 and 5 min with 0.25 ml of ice-cold Na_2CO_3 solution (final pH 11). Incubations using 0.1 mg/ml HLMs with and without NADPH at 0 and 5 min served as positive and negative controls, respectively. Following the addition of 50 μl of the internal standards ($^{15}N_3$-labeled 1′-OH MDZ and 4′-OH MDZ), samples were briefly vortexed and 3 ml ethyl acetate was added. Samples were then horizontally shaken for 20 min and centrifuged at 3700 × *g* for 20 min at room temperature. The supernatant was evaporated in a 37 °C water bath with nitrogen gas. Residues were finally resuspended in 200 μl of 50:50 acetonitrile:water, 100 μl was transferred to a 96-well plate, and 10 μl was injected for analysis by HPLC-MS/MS. Duplicate determinations were performed for each sample. Under these conditions, the depletion of MDZ did not exceed 20%.

1′-OH and 4′-OH MDZ concentrations were quantified by HPLC-MS/MS using an Agilent series 1290 HPLC interfaced with an Agilent 6410B triple quadrupole mass spectrometer (Agilent Technologies, Palo Alto, CA). Separation of 1′-OH and 4′-OH MDZ was achieved using a Zorbax SB-C18 column (150 mm × 2.1 mm × 5 μ) heated to 35 °C. Metabolites were separated with isocratic elution: 35% mobile phase B from 0–6 min, followed by 95% B at 6–9 min for column rinsing, and finally returned to 35% for the remainder of the 14 min run time. The mass spectrometer was run in ESP positive ionization mode with a capillary voltage of 1800 V and a fragmentation voltage of 150, 145, and 152 V for the internal standard, 1′-OH MDZ, and 4′-OH MDZ, respectively. The drying gas temperature was 350 °C, the nitrogen drying gas flow rate was 11.0 L/min, and the nebulizer pressure was 35 pound-force per square-inch-gauge. The following ion transitions were monitored: *m/z* 342.1 > 324.1 for 1′-OH MDZ, *m/z* 342.1 > 297.1 for 4′-OH MDZ, and *m/z* 347.1 > 329.2 for internal standards.

2.9. Glyburide fraction unbound in CYP supersomes and HFLMs

Protein binding of glyburide in CYP3A4, CYP3A5, and CYP3A7 supersomes as well as HFLMs and HLMs was determined by ultrafiltration using Microcon-10 kDa Centrifugal Filters with Ultracel-10 membranes (EMD Millipore Corporation, Billerica, MA). [^{3}H]-Glyburide (~1.5 ng) in methanol was aliquoted into 1.5 ml eppendorf tubes and evaporated to dryness. [^{3}H]-Glyburide was reconstituted in 100 mM potassium phosphate buffer (1 mM EDTA, pH7.4) containing varying concentrations of glyburide (0.01, 0.05, and 20 μM) and protein concentrations identical to those used in depletion studies, in a total volume of 350 μl. Samples were briefly vortexed, and aliquots (110 μl) were transferred to ultrafiltration cartridges, equilibrated for 30 min at 37 °C, and centrifuged at 1000 × *g* for 10 min. Eight microliters of filtrate and unfiltered samples were counted on a liquid scintillation counter. The fraction unbound (f_u) of glyburide was calculated as the percentage of radioactivity of the filtrate to the radioactivity of the corresponding unfiltered incubation buffer/protein mixture. Triplicate determinations were performed for each sample. HLMs served as a positive control. Incubation buffer was used to determine non-specific binding of [^{3}H]-glyburide, which was 6.9 ± 3.7% (*n* = 9 replicates).

3. Results

3.1. Glyburide depletion kinetics of CYP3A supersomes

We first compared the kinetics of glyburide metabolism with recombinant CYP3A4, CYP3A5 and CYP3A7 supersomes. Substrate depletion kinetic parameters were estimated and the data are shown in Table 2. The kinetic profiles from a representative experiment are depicted in Fig. 1. K_m and V_{max} values were estimated from three independent experiments. The fraction unbound (f_u) remained constant for each CYP3A isoform over 0.01–20 μM glyburide. The f_u was 5–7% for CYP3A4 and CYP3A7 and

Table 2
Glyburide depletion kinetics in CYP3A supersomes.

	$K_{m,\ app}$ (μM)	$K_{m,\ u}$ (μM)	V_{max} (nmol/min/nmol P450)	$Cl_{int,\ u}$ (ml/min/nmol P450)	fu (%)
CYP3A4	3.1 ± 1.1	0.22 ± 0.08[a]	8.3 ± 4.8	37.1 ± 13.1[a,c]	7.1 ± 6.1
CYP3A5	3.0 ± 0.1	0.41 ± 0.01[a,b]	3.6 ± 0.3	8.7 ± 0.5[a]	13.6 ± 4.2[d]
CYP3A7	2.6 ± 0.9	0.15 ± 0.05[b]	1.8 ± 0.6	13.0 ± 3.0[c]	5.7 ± 3.9[d]

[a] $p < 0.05$ between CYP3A4 and CYP3A5.
[b] $p < 0.01$ between CYP3A5 and CYP3A7.
[c] $p < 0.05$ between CYP3A4 and CYP3A7.
[d] $p < 0.05$ between CYP3A5 and CYP3A7; Shown are means ± SD of three independent experiments. Fraction unbound (fu) is reported as mean ± SD (*n* = 6). $K_{m,\ app}$ represents K_m apparent; $K_{m,\ u}$ represents K_m unbound; $Cl_{int,\ u}$ represents unbound intrinsic clearance.

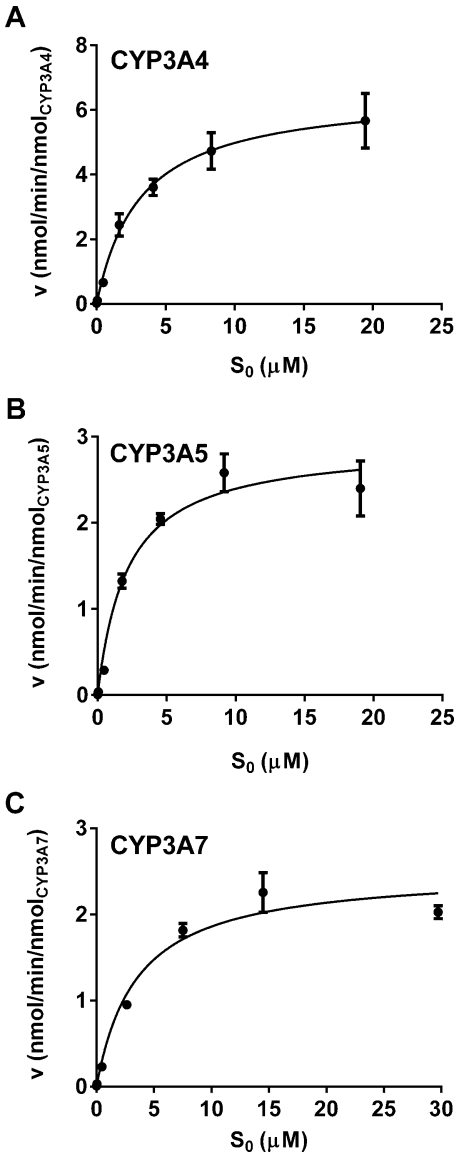

Fig. 1. Representative kinetic profiles of glyburide depletion velocity versus initial glyburide concentration in CYP3A4 (A), CYP3A5 (B), and CYP3A7 (C) supersomes. Shown are means ± SD of three replicate determinations per time point in a representative experiment. S_0, initial substrate (glyburide) concentration at time zero.

~15% for CYP3A5 (Table 2). Although apparent K_m values ($K_{m,\ app}$) did not significantly differ between CYP3A isoforms, K_m values corrected for protein binding ($K_{m,\ u}$) did, with CYP3A7 having the highest affinity to glyburide (in the nM range), followed by CYP3A4 and CYP3A5. CYP3A4 had the highest capacity to metabolize glyburide (V_{max} = 8.3 nmol/min/nmol P450), followed by CYP3A5 and CYP3A7 (V_{max} = 3.6 and 1.8 nmol/min/nmol P450, respectively). Consequently, $Cl_{int,\ u}$ of CYP3A4 was nearly 3-fold greater than that of CYP3A7 and 4-fold greater than that of CYP3A5 (37.1 versus 13.0 and 8.7 ml/min/nmol P450, respectively).

3.2. Human fetal liver demographics and CYP protein quantification

Estimated gestational age, fetal sex, race, post-mortem interval (time between death and tissue collection), genotype, and maternal medications or xenobiotics are listed for sixteen human fetal livers in Table 3. Nearly equal numbers of male and female fetal livers were collected (7 and 9, respectively). Estimated gestational age spanned from 13 to 21 weeks of gestation; however, most fetal livers were between the ages of 13 and 16 weeks of gestation. The composition of races among the fetal livers that were collected nearly reflects the composition of the population within the state of Washington. The top three maternal medications or xenobiotics recorded were alcohol, cigarettes, and marijuana. *CYP3A5*3/*3* and *CYP3A7*1/*1* were the most abundant variant CYP3A genotypes. Of the CYP isoforms quantified by HPLC-MS/MS, only CYP3A7 and P450 reductase were detected in quantifiable amounts; however multiple CYP isoforms were detected in pooled HLM quality controls. The CYP3A7 protein levels in HFLMs ranged between 10 and 160 pmol/mg protein (Fig. 2). CYP3A5 protein was detectable in some of the HFLMs, but was not quantifiable due to a somewhat high LLOQ (lower limit of quantification), (0.475 fmol/μg microsomal protein). The relationship between selected demographics and human fetal liver CYP3A7 protein levels was explored (Fig. 2). CYP3A7 content did not appear to be sex-dependent, or affected by *CYP3A7*1C* and **2C* genotype (p = 0.45 and 0.40, respectively) (Fig. 2). Given the small estimated gestational age range of the human fetal livers, it was not possible to evaluate the relationship between CYP3A7 protein content and gestational age or post-mortem intervals (all less than 6 h) (Fig. 2). Overall, none of these potential effectors significantly influenced protein levels of CYP3A7 in the human fetal liver samples of this study.

Table 3
Demographics of human fetal livers.

ID	EGA (wk)	Sex	Race	PMI (h)	CYP3A5 genotype	CYP3A7 genotype	Maternal medications
25423	13	F	H	Unk	*3/*3	*1/*1	Unk
25421	13	F	CA	3:20	*3/*3	*1/*1	Alcohol, cigarettes
25422	13	F	NA	2:37	*1/*1	*1/*2C	Alcohol, cigarettes, marijuana
25448	13	M	Unk	Unk	*3/*6	*1/*2C	Unk
25458	14	M	CA	> 24:00	*1/*3	*1/*1	Alcohol, cigarettes, marijuana
25351	15	M	CA	6:13	*3/*3	*1/*1	Alcohol, levothyroxine
25279	15	M	PI, S	3:08	*1/*3	*1/*2C	Alcohol
25346	15	F	H	2:10	*3/*6	*1/*1C	Albuterol, alcohol, cigarettes, crystal methamphetamine, marijuana, acetaminophen/hydrocodone
25452	15	F	CA	2:38	*1/*3	*1/*2C	Unk
25217	15	F	AA, H	21:00	*1/*6	*1/*2C	Unk
25435	15	F	CA, EI	1:07	*3/*3	*1/*1	Alcohol, cigarettes, crystal methamphetamine
25447	15	M	CA	4:36	*3/*3	*1/*1	Cigarettes
25449	15	F	CA	2:22	*3/*3	*1/*1	Ibuprofen, marijuana
25453	15	M	CA	5:20	*3/*3	*1/*1	Alcohol, ibuprofen, marijuana
25388	16	F	CA, H	Unk	*3/*3	*1/*1	Cigarettes, ibuprofen, marijuana, prenatal vitamins
25212	21	M	CA	5:15	*1/*3	*1C/*2C	Alcohol, birth control pill, amphetamine/dextroamphetamine

EGA, estimated gestational age; Unk, unknown; H, Hispanic; CA, Caucasian; NA, Native American; PI, Pacific Islander; S, Samoan; AA, African-American; EI, East Indian; PMI, post-mortem interval.

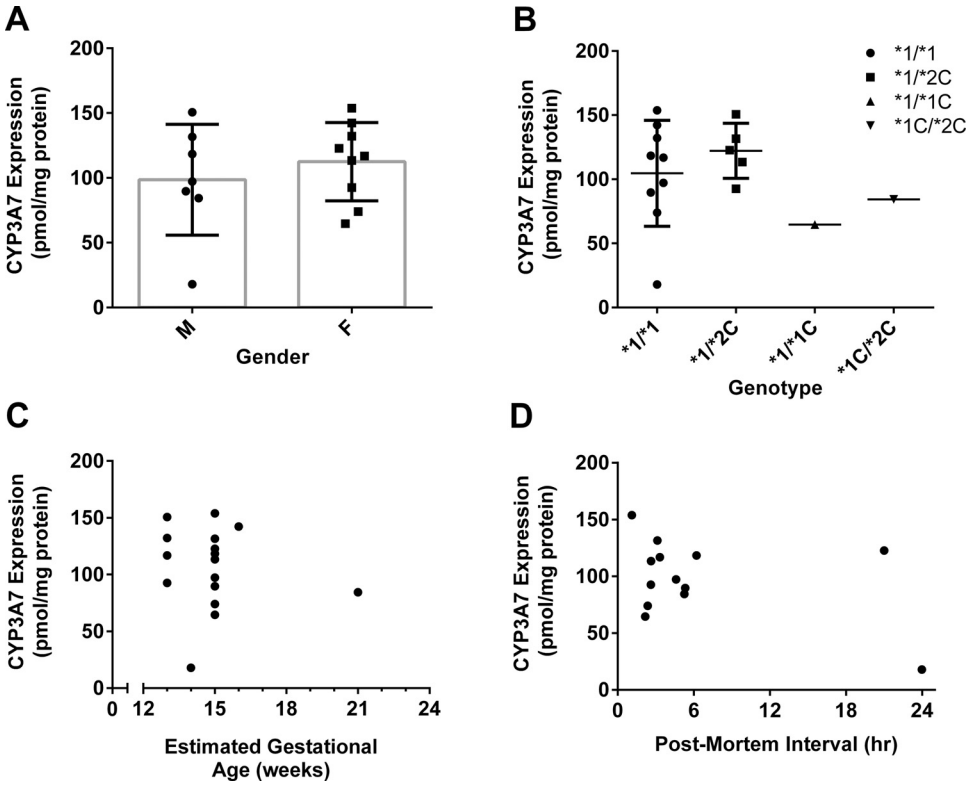

Fig. 2. Effects of gender (A), CYP3A7 genotype (B), estimated gestational age (C), and post-mortem interval (D) on CYP3A7 protein content in sixteen human fetal livers. Protein levels are shown as means of triplicate determinations from a single experiment. Using an unpaired Student's *t*-test ($p < 0.05$), no statistically significant differences in CYP3A7 protein levels were observed based upon gender ($p = 0.45$) or CYP3A7 genotype ($p = 0.40$). Statistical analyses were performed using the Graphpad Prism version 6.04 software.

3.3. Metabolic profiles of glyburide generated by CYP3A supersomes, HFLMs, and HLMs

The primary metabolites of glyburide, M1–M5, are all monohydroxylated metabolites. Given the same CYP3A isoform concentration (30 pmol/ml), M5 was the dominant metabolite formed (of the metabolites measured) following a 30 min incubation with CYP3A4, CYP3A5 or CYP3A7 supersomes, the relative abundance of which was approximately 73, 57, and 96%, respectively (Fig. 3, Table 4). Differences were observed between the relative abundance of M1-M5 across CYP3A isoforms. M5 appears to be predominant metabolite for all three CYP3A isoforms (57–96%); however, CYP3A7 produced ≤1% M1–M4 which was far less than 5–15% of M1–M4 formed by CYP3A4 or CYP3A5. The relative abundance of M1–M5 in CYP3A supersomes was independent of incubation time (30–90 min) and glyburide concentration (0.05–20 μM) (data not shown). With the same protein concentration (0.8 mg/ml), pooled HFLMs and pooled HLMs also predominantly formed M5 (97.0 and 64.9%, respectively) (Fig. 4, Table 4). Interestingly, the metabolite profile in pooled HFLMs mirrored the profile generated by CYP3A7. On the other hand, the metabolic profile from pooled HLMs mirrored that from CYP3A4 (Figs. 3 and 4). However, the relative abundance of M1 in pooled HLMs on average was higher (~10%) than that in CYP3A4 or CYP3A5 (~5%). Again, the relative abundance of M1-M5 in HFLMs was not dependent on incubation time (30–90 min) or glyburide concentration (0.05–20 μM) (data not shown).

3.4. Correlation of glyburide depletion in HFLMs with CYP3A7 protein content, 16α-OH DHEA formation, and 4′-OH MDZ formation

Since M5 was the predominate metabolite formed by HFLMs, which cannot be quantified due to lack of commercially available standard, glyburide depletion was performed to estimate glyburide Cl_{int} in individual HFLMs (depletion curves not shown). Glyburide depletion in HFLMs was NADPH-dependent, supporting the hypothesis that CYP3A7 in the fetal liver is the predominant enzyme responsible for glyburide metabolism. The average fraction unbound of glyburide across all sixteen HFLMs was 27.0 ± 7.9% ($n = 3$ replicates per liver) compared to 17.4 ± 1.4% ($n = 3$) in pooled HLMs ($p = 0.055$). In order to confirm that fetal CYP3A7 protein content in HFLMs was indeed correlated with CYP3A7 activity, DHEA metabolism to 16α-OH DHEA (a reaction specific to CYP3A7) was measured. We found that CYP3A7 protein levels were indeed highly correlated with 16α-OH DHEA formation (Pearson $r = 0.76$, $p < 0.001$) (Fig. 5, panel A). CYP3A7 protein levels were also tightly correlated with Cl_{int} for glyburide depletion (Pearson $r = 0.80$, $p < 0.001$) (Fig. 5, panel B), supporting the hypothesis that glyburide is primarily metabolized by CYP3A7 in human fetal livers. Fig. 5C also shows that glyburide depletion is directly correlated with 16α-OH DHEA formation (Pearson $r = 0.80$, $p < 0.001$). Midazolam, a probe CYP3A substrate, was also used to discern CYP3A7 activity. 1′-OH MDZ formation was moderately correlated with Cl_{int} for glyburide depletion (Pearson $r = 0.52$, $p = 0.037$) (Fig. 6A), while 4′-OH MDZ formation was highly correlated with glyburide Cl_{int} (Pearson $r = 0.89$, $p < 0.001$) (Fig. 6B) as well as CYP3A7 protein levels (Pearson $r = 0.68$, $p = 0.004$) (Fig. 6C). There was no correlation between the 1′-OH/4′-OH metabolite ratio and glyburide Cl_{int} (data not shown).

3.5. Glyburide depletion is not dependent on CYP3A5 genotype

We also examined whether CYP3A5 genotype impacts glyburide depletion and found that CYP3A5 genotype did not affect glyburide Cl_{int} or 16α-OH DHEA formation (Fig. 7, panels A and B). The 1′-OH/4′-OH MDZ metabolite ratio was nearly two-fold larger for the single homozygous *CYP3A5*1/*1* expresser compared to the heterozygous (*CYP3A5*1/*3* and *CYP3A5*1/*6*) and homozygous (*CYP3A5*3/*3*, *CYP3A5*3/*6*, and *CYP3A5*6/*6*) variant genotypes,

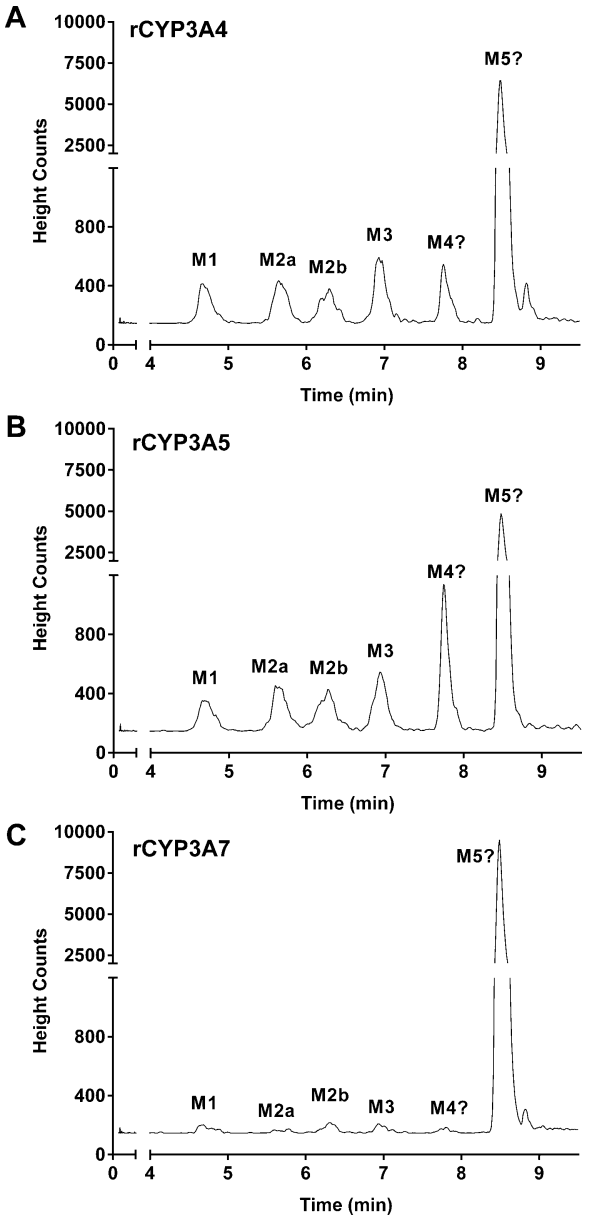

Fig. 3. Representative metabolite profile of glyburide in CYP3A4 (A), CYP3A5 (B), and CYP3A7 (C) supersomes. Mass ion chromatograms for extracts of supersome incubates showing the presence of the following metabolites: M1, M2a, M2b, M3, M4, and M5.

which are associated with decreased CYP3A5 protein levels [40] (Fig. 7, panel C). Due to only one sample with the CYP3A5*1/*1 genotype, statistical analyses between groups was not performed.

Table 4
Relative distribution (%) of glyburide's metabolic profile in CYP3A supersomes, HFLMs, and HLMs.

	M1	M2a	M2b	M3	M4	M5
CYP3A4[a]	5.0 ± 1.2	5.6 ± 1.2	4.6 ± 1.3	7.4 ± 1.3	4.8 ± 1.1	72.6 ± 6.2
CYP3A5[a]	5.6 ± 0.3	8.0 ± 0.4	7.4 ± 0.8	8.6 ± 0.3	13.5 ± 0.9	57.0 ± 2.1
CYP3A7[a]	1.1 ± 0.05	0.5 ± 0.02	1.0 ± 0.1	1.0 ± 0.1	0.4 ± 0.2	96.1 ± 0.3
HFLM[b]	1.2 ± 0.4	0.2 ± 0.2	0.7 ± 0.3	0.9 ± 0.3	0.05 ± 0.2	97.0 ± 0.9
HLM[c]	10.5 ± 0.4	7.0 ± 0.5	6.0 ± 0.4	7.3 ± 0.4	4.4 ± 0.5	64.9 ± 0.8

[a] Shown are means ± SD of CYP3A supersomes measured in duplicate from two separate experiments.
[b] sixteen human fetal livers measured in duplicate from one experiment.
[c] pooled human liver microsomes measured in duplicate from two experiments.

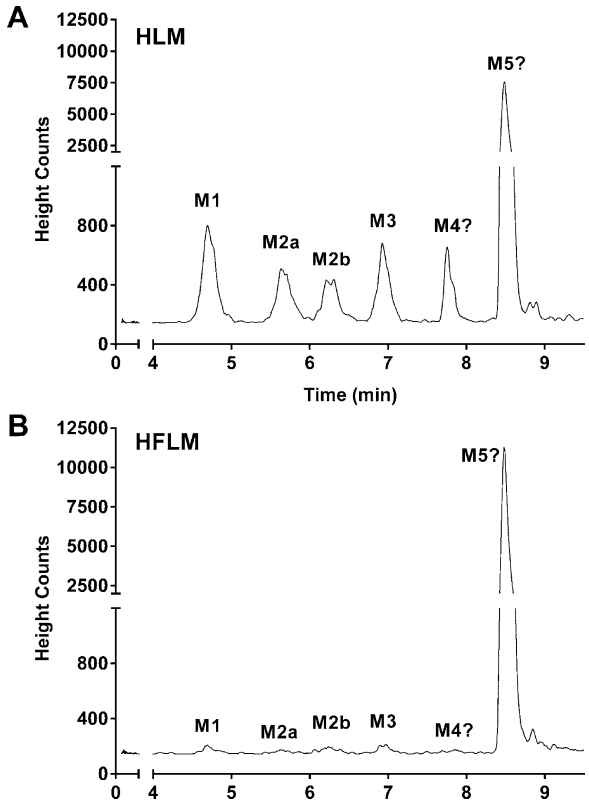

Fig. 4. Representative metabolic profile of glyburide in human liver microsomes (A) and human fetal liver microsomes (B). Mass ion chromatograms for extracts of supersome incubates showing the presence of the following metabolites: M1, M2a, M2b, M3, M4, and M5.

4. Discussion

Glyburide is frequently used to treat GDM. However, a major concern of pregnant women using glyburide is the safety of the drug for the developing fetus. It is critical that we understand the mechanisms that control fetal exposure to glyburide, such as placental penetration and placental and fetal metabolism of glyburide. Previous studies including those from our laboratory have identified that ABC transporters such as BCRP play an important role in limiting transfer of glyburide across the placenta [16–18]. Placental metabolism of glyburide primarily by CYP19 has also been demonstrated [9,10,19]. Prior to this work, no studies have been done to evaluate fetal metabolism of glyburide. Thus, the purpose of this study was to systematically investigate glyburide metabolism by human fetal livers.

Since CYP3A7 is known to be the predominant drug-metabolizing CYP enzyme in human fetal livers [21–23], we first characterized glyburide depletion kinetics of CYP3A7 supersomes and compared the data with those of CYP3A4 and CYP3A5 (Fig. 1 and Table 2). CYP3A7 was able to catalyze glyburide depletion but with a relative lower (~65%) efficiency than CYP3A4. The $K_{m,\,u}$ values of CYP3A4 and CYP3A7 after correction for protein binding were comparable; however, the V_{max} of CYP3A4 was 4-5 times greater than that of CYP3A7, resulting in a nearly 3-fold difference in $Cl_{int,\,u}$ (Table 2). On the other hand, the $Cl_{int,\,u}$ values of CYP3A5 and CYP3A7 were similar. Given the lower $Cl_{int,\,u}$ of CYP3A7 versus CYP3A4, quantifying CYP3A7 protein levels in human fetal livers is important in the effort to determine the overall contribution of CYP3A7 to glyburide metabolism in human fetal livers.

Thus, we performed absolute quantification of CYP enzymes in 16 individual HFLMs using a targeted mass spectrometry approach. Of the enzymes examined: CYP3A4, CYP3A5, CYP3A7,

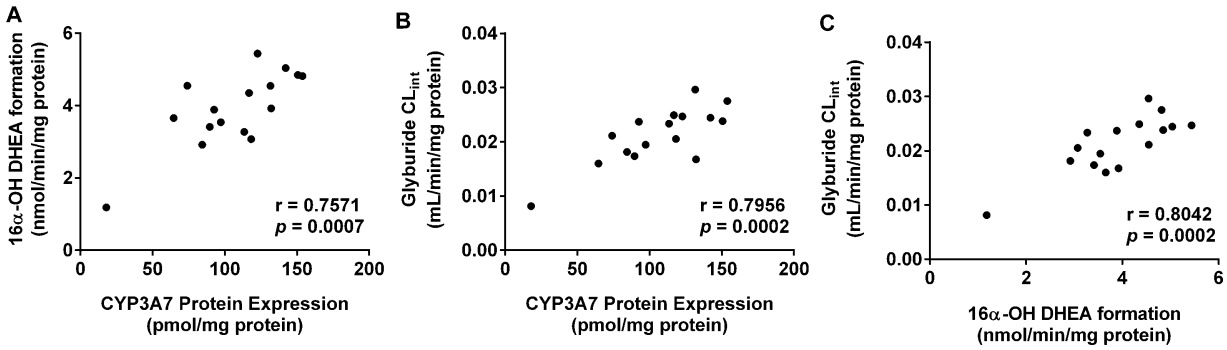

Fig. 5. Correlation between CYP3A7 protein content and 16α-OH DHEA formation (A) or Cl_{int} of glyburide depletion (B), as well as correlation between Cl_{int} of glyburide depletion and 16α-OH DHEA formation (C) in human fetal liver microsomes. Shown are means of duplicate incubations from single experiments. Statistically significant correlations ($p < 0.001$) were determined by the Pearson correlation analysis using the Graphpad Prism version 6.04 software.

CYP2C9, CYP2C19, CYP2A6, and CYP2D6, only CYP3A7 protein levels were quantifiable in HFLMs. CYP3A5 was detectable in some of the HFLMs, but not quantifiable due to a somewhat high LLOQ. Other CYPs were not detectable at all. These results suggest that CYP3A7 is likely the major enzyme capable of metabolizing glyburide in human fetal livers, even if it has a relatively lower $Cl_{int, u}$ compared to CYP3A4. We noted that CYP3A7 protein levels in individual HFLMs were only slightly variable, ranging from approximately 50–160 pmol/mg protein with only one sample at around 10 pmol/mg protein (Fig. 2). The protein levels of CYP3A7 in human fetal livers are in a similar range to the protein levels of CYP3A4 in human adult livers, but are much higher than those of CYP3A5 (up to 20 pmol/mg protein) [41]. Thus, CYP3A7 could significantly contribute to drug metabolism in human fetal livers, affecting fetal exposure to drugs. This study is the first to report CYP3A7 protein quantification by surrogate peptide-based HPLC-MS/MS in individual human fetal livers. The fetal livers were collected from women using medications and other substances. Alcohol, marijuana and cigarettes were the three most common substances used, though they did not seem to affect CYP3A7 microsomal protein levels. CYP3A7 protein content also did not seem to be affected by sex of the fetus, CYP3A7 genotype, estimated gestational age, or post-mortem interval (Fig. 2). One fetal liver (ID# 25458) had a post-mortem interval of >24 hours and showed a notably lower level of CYP3A7 protein content (Fig. 2). It is possible that the longer post-mortem interval would leave time for protein degradation to occur, and ultimately decrease CYP3A7 protein levels. Other factors may also play a role as another fetal liver (ID# 25217) with a post-mortem interval of 21 h possessed CYP3A7 protein levels comparable to other fetal livers with much shorter post-mortem intervals.

We then characterized the metabolic profiles of glyburide by CYP3A4, CYP3A5, CYP3A7, HFLMs, and HLMs. M5 was the predominant metabolite (of the metabolites measured) by CYP3A4, CYP3A5, and CYP3A7 with a relative abundance of 60-70% for CYP3A4 or CYP3A5 and of 96% for CYP3A7 (Fig. 3 and Table 4). Likewise, of the metabolites measured, M5 accounted for nearly 97.0% of relative abundance in HFLMs versus 64.9% in HLMs (Fig. 4 and Table 4). This pattern of metabolic profile again supports the notion that CYP3A7 is likely the major enzyme in human fetal livers responsible for glyburide metabolism. In a previous clinical study, steady-state concentrations of glyburide in women with GDM were reported to range from 3 nM to 250 nM over a 12-h dosing interval [11]. These concentrations are well below the apparent K_m of CYP3A7 but similar to its $K_{m, u}$. As glyburide can cross the placenta and reach umbilical cord concentrations that are 70% of maternal concentrations at term [11], we anticipate that the predominant metabolite of glyburide produced by human fetal livers would be M5, followed by minimal levels of M1–M4. Extrahepatic fetal metabolism and placental metabolism may also influence the overall fetal metabolism and metabolite profile of glyburide in the fetus. Fetal adrenal metabolism has been reported for endogenous compounds such as testosterone [42]. CYP3A7 activity in fetal adrenal microsomes was evaluated via testosterone metabolism to 6β-OH testosterone; 6β-OH formation was 33% of that measured in fetal liver microsomes with matched tissues between 24–39 weeks of gestation [43]. Thus, fetal adrenal metabolism of glyburide by CYP3A7 may also contribute to overall fetal metabolism of glyburide, but is not expected to change the metabolite profile of glyburide in the fetus. Human term placenta has also been shown to metabolize glyburide, predominantly to M5 via CYP19 [9,10,20]. If M5 formed in the placenta can access the fetal circulation, placental metabolism could alter the overall metabolic profile of glyburide in the fetus. Although M5 is a major metabolite of both fetal and placental metabolism of glyburide, whether it is pharmacologically active is not known. This would be

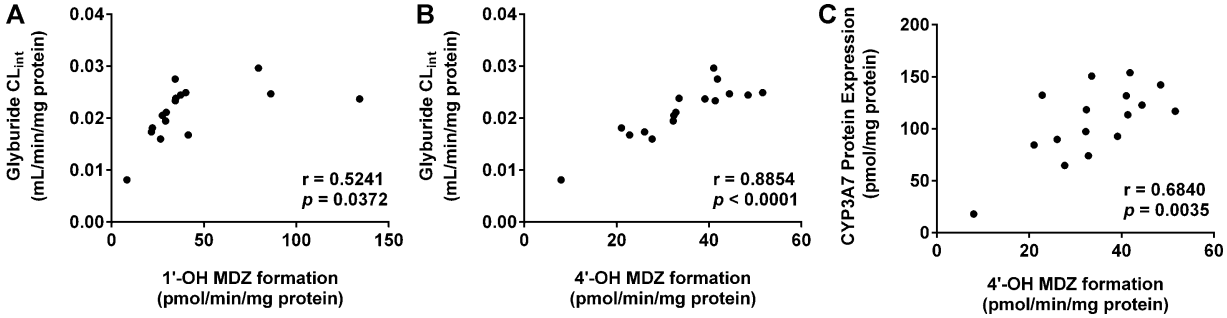

Fig. 6. Glyburide Cl_{int} is correlated with 4′-OH midazolam formation in HFLMs. Shown are means of duplicate incubations from single experiments. Statistically significant correlations ($p < 0.05$) between glyburide Cl_{int} and 1′-OH midazolam formation (A), 4′-OH midazolam formation (B), as well as correlations between CYP3A7 protein content and 4′-OH midazolam (C) were determined by the Pearson correlation analysis using the Graphpad Prism version 6.04 software.

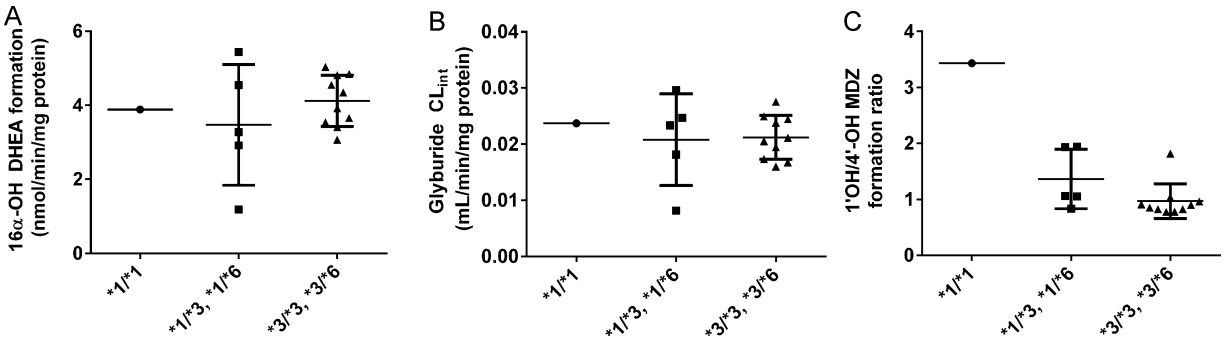

Fig. 7. Effects of CYP3A5 genotype on 16α-OH DHEA formation (A), glyburide Cl_{int} (B), and 1′-OH/4′-OH midazolam formation ratios (C) in HFLMs. Shown are means of duplicate incubations from single experiments.

of considerable importance to investigate in future studies given that the other metabolites, M1 and M2b, are pharmacologically active [30].

After having established that CYP3A7 and HFLMs are capable of metabolizing glyburide, we performed further studies to confirm that CYP3A7 is the major enzyme in HFLMs responsible for glyburide metabolism using selective probe substrates. First of all, with 16 individual HFLMs, we found that 16α-OH DHEA formation, a reaction specific to CYP3A7, was highly correlated with CYP3A7 protein levels (Fig. 5A). Glyburide Cl_{int} was highly correlated with CYP3A7 protein levels (Fig. 5B) and 16α-OH DHEA formation (Fig. 5C), supporting the conclusion that CYP3A7 is the enzyme responsible for glyburide metabolism in HFLMs.

We noted that HFLMs were also capable of metabolizing MDZ (Fig. 6A and B). It has been reported that the K_m values of CYP3A4 for 1′-OH MDZ and 4′-OH MDZ formation differ by a magnitude of 10 (2–6 μM versus 40–60 μM, respectively) [41]. The starting MDZ concentration in our incubations with HFLMs was 8 μM; therefore, if CYP3A4 or CYP3A5 were expressed in HFLMs, we might expect preferential formation of 1′-OH MDZ and the corresponding 1′-OH/4′-OH metabolite ratio to be far greater than 1. The metabolite ratio, however, was less than or around unity for 12 out of the 16 HFLMs (Fig. 7C), suggesting that CYP3A4 may not expressed in this set of fetal livers. In addition, glyburide Cl_{int} (Fig. 6B) and CYP3A7 protein content (Fig. 6C) were highly correlated with 4′-OH MDZ formation, confirming that CYP3A7 can catalyze 4′-OH MDZ formation. Considering CYP3A7's perhaps preferential formation of 4′-OH MDZ (given the MDZ incubation concentration used), and the fact that CYP3A5 protein was not quantifiable in these HFLMs, it is understandable why the 1′-OH/4′-OH MDZ ratio was $\leq$1 for the majority of HFLMs. For the metabolite ratios that were >1, CYP3A5 was likely present to a sufficient degree to form more 1′-OH MDZ, thus changing the metabolite ratio. The highest observed 1′-OH/4′-OH ratio (3.4) came from a fetal liver with the CYP3A5*1/*1 genotype, which is associated with expression of functional CYP3A5 (Fig. 7C). This supports the likelihood that CYP3A5 is present in some HFLMs and plays a role in the fetal metabolism of MDZ. The results of midazolam metabolism provide further evidence that CYP3A7 is the major CYP3A isoform in the fetal liver, and that CYP3A7 preferentially oxidizes substrates at sites that may be different from that of other CYP3A isoforms.

16α-OH DHEA formation was unaffected by CYP3A5 genotype (Fig. 7A), which is expected because 16α-OH DHEA formation is specific to CYP3A7 [20]. Given the low concentration of glyburide used in correlation studies (0.05 μM) and that the $K_{m,u}$ of CYP3A7 for glyburide is 2–3 times lower than that of CYP3A5 (Table 2), contribution of CYP3A5 to glyburide depletion would perhaps be unobservable. Therefore, glyburide Cl_{int} was not affected by *CYP3A5* genotype either. Given the low content of CYP3A5 in human fetal livers, contribution of CYP3A5 to fetal liver metabolism of glyburide is expected to be much lower than CYP3A7.

In summary, we have shown that CYP3A7 is substantially expressed in in human fetal livers and for the first time mediates metabolism of glyburide to the primary metabolite M5. Microsomal CYP3A7 protein content in human fetal livers was not affected by sex of the fetus, genotype, or gestational age, and correlated well with glyburide Cl_{int}, 16α-OH DHEA formation, and 4′-OH MDZ formation. These results are of significant clinical value for understanding and predicting fetal exposure to glyburide and informing fetal safety of the drug.

Acknowledgements

We greatly acknowledge Drs. Abhinav Nath and Laura Shireman for their discussions and expertise regarding substrate depletion experimental design and data analysis. This study was supported in part by the Eunice Kennedy Shriver National Institute of Child Health & Human Development (NICHD) [Grant U10HD047892] and the National Center for Advancing Translational Sciences (NCATS) [Grant TL1 RR025016]. The content is solely the responsibility of the authors and does not necessarily represent the official views of the NICHD, NCATS, or the National Institutes of Health. The authors would also like to acknowledge funding support from UWRAPT (http://sop.washington.edu/uwrapt) for CYP protein quantification. Diana Shuster is the recipient of the American Foundation for Pharmaceutical Education Pre-doctoral Fellowship in Pharmaceutical Sciences.

References

[1] Paglia MJ, Coustan DR. Gestational diabetes: evolving diagnostic criteria. Curr.Opin. Obstet. Gynecol. 2011;23:72–5.
[2] Jovanovic L, Pettitt DJ. Gestational diabetes mellitus. JAMA 2001;286:2516–8.
[3] Camelo Castillo W, Boggess K, Sturmer T, Brookhart MA, Benjamin Jr DK, Jonsson Funk M. Trends in glyburide compared with insulin use for gestational diabetes treatment in the United States, 2000–2011. Obstet.Gynecol. 2014;123:1177–84.
[4] Coetzee EJ, Jackson WP. The management of non-insulin-dependent diabetes during pregnancy. Diabetes Res Clin.Pract. 1985;1:281–7.
[5] Bertini AM, Silva JC, Taborda W, Becker F, Lemos Bebber FR, Zucco Viesi JM, et al. Perinatal outcomes and the use of oral hypoglycemic agents. J.Perinat. Med. 2005;33:519–23.
[6] Langer O, Conway DL, Berkus MD, Xenakis EM, Gonzales O. A comparison of glyburide and insulin in women with gestational diabetes mellitus. New Engl. J. Med. 2000;343:1134–8.
[7] Anjalakshi C, Balaji V, Balaji MS, Seshiah V. A prospective study comparing insulin and glibenclamide in gestational diabetes mellitus in Asian Indian women. Diabetes Res.Clin. Pract. 2007;76:474–5.
[8] Ogunyemi D, Jesse M, Davidson M. Comparison of glyburide versus insulin in management of gestational diabetes mellitus. Endocr.Pract. 2007;13:427–8.
[9] Zharikova OL, Fokina VM, Nanovskaya TN, Hill RA, Mattison DR, Hankins GD, et al. Identification of the major human hepatic and placental enzymes responsible for the biotransformation of glyburide. Biochem.Pharmacol. 2009;78:
1483–90.
[10] Ravindran S, Zharikova OL, Hill RA, Nanovskaya TN, Hankins GD, Ahmed MS. Identification of glyburide metabolites formed by hepatic and placental microsomes of humans and baboons. Biochem.Pharmacol. 2006;72:1730–7.

[11] Hebert MF, Ma X, Naraharisetti SB, Krudys KM, Umans JG, Hankins GD, et al. Are we optimizing gestational diabetes treatment with glyburide? The pharmacologic basis for better clinical practice. Clin.Pharmacol. Ther. 2009;85:607–14.
[12] Behravan J, Piquette-Miller M. Drug transport across the placenta, role of the ABC drug efflux transporters. Expert Opin.Drug Metab. Toxicol. 2007;3:819–30.
[13] Mao Q. BCRP/ABCG2 in the placenta: expression, function and regulation. Pharm.Res. 2008;25:1244–55.
[14] Ceckova-Novotna M, Pavek P, Staud F. P-glycoprotein in the placenta: expression, localization, regulation and function. Reprod.Toxicol. 2006;22:400–10.
[15] Ni Z, Mao Q. ATP-binding cassette efflux transporters in human placenta. Curr.Pharm. Biotechnol. 2011;12:674–85.
[16] Zhou L, Naraharisetti SB, Wang H, Unadkat JD, Hebert MF, Mao Q. The breast cancer resistance protein (Bcrp1/Abcg2) limits fetal distribution of glyburide in the pregnant mouse: an Obstetric-Fetal Pharmacology Research Unit Network and University of Washington Specialized Center of Research Study. Mol.Pharmacol. 2008;73:949–59.
[17] Gedeon C, Behravan J, Koren G, Piquette-Miller M. Transport of glyburide by placental ABC transporters: implications in fetal drug exposure. Placenta 2006;27:1096–102.
[18] Hemauer SJ, Patrikeeva SL, Nanovskaya TN, Hankins GD, Ahmed MS. Role of human placental apical membrane transporters in the efflux of glyburide, rosiglitazone, and metformin. Am.J. Obstet. Gynecol. 2010;202:383 e1–3837e.
[19] Zharikova OL, Ravindran S, Nanovskaya TN, Hill RA, Hankins GD, Ahmed MS. Kinetics of glyburide metabolism by hepatic and placental microsomes of human and baboon. Biochem.Pharmacol. 2007;73:2012–9.
[20] Jain S, Zharikova OL, Ravindran S, Nanovskya TN, Mattison DR, Hankins GD, et al. Glyburide metabolism by placentas of healthy and gestational diabetics. Am.J. Perinatol. 2008;25:169–74.
[21] Komori M, Nishio K, Kitada M, Shiramatsu K, Muroya K, Soma M, et al. Fetus-specific expression of a form of cytochrome P-450 in human livers. Biochemistry 1990;29:4430–3.
[22] Leeder JS, Gaedigk R, Marcucci KA, Gaedigk A, Vyhlidal CA, Schindel BP, et al. Variability of CYP3A7 expression in human fetal liver. J.Pharmacol. Exp. Ther. 2005;314:626–35.
[23] Hakkola J, Raunio H, Purkunen R, Saarikoski S, Vahakangas K, Pelkonen O, et al. Cytochrome P450 3A expression in the human fetal liver: evidence that CYP3A5 is expressed in only a limited number of fetal livers. Biol.Neonate 2001;80:193–201.
[24] Schuetz JD, Beach DL, Guzelian PS. Selective expression of cytochrome P450 CYP3A mRNAs in embryonic and adult human liver. Pharmacogenetics 1994;4:11–20.
[25] Zhou L, Naraharisetti SB, Liu L, Wang H, Lin YS, Isoherranen N, et al. Contributions of human cytochrome P450 enzymes to glyburide metabolism. Biopharm.Drug Dispos. 2010;31:228–42.
[26] Chen H, Fantel AG, Juchau MR. Catalysis of the 4-hydroxylation of retinoic acids by cyp3a7 in human fetal hepatic tissues. Drug Metab.Dispos. 2000;28:1051–7.
[27] Shimada T, Yamazaki H, Mimura M, Wakamiya N, Ueng YF, Guengerich FP, et al. Characterization of microsomal cytochrome P450 enzymes involved in the oxidation of xenobiotic chemicals in human fetal liver and adult lungs. Drug Metab.Dispos. 1996;24:515–22.
[28] Yang HY, Lee QP, Rettie AE, Juchau MR. Functional cytochrome P4503A isoforms in human embryonic tissues: expression during organogenesis. Mol.-Pharmacol. 1994;46:922–8.
[29] Gedeon C, Anger G, Piquette-Miller M, Koren G. Breast cancer resistance protein: mediating the trans-placental transfer of glyburide across the human placenta. Placenta 2008;29:39–43.
[30] Rydberg T, Jonsson A, Roder M, Melander A. Hypoglycemic activity of glyburide (glibenclamide) metabolites in humans. Diabetes Care 1994;17:1026–30.
[31] Paine MF, Khalighi M, Fisher JM, Shen DD, Kunze KL, Marsh CL, et al. Characterization of interintestinal and intraintestinal variations in human CYP3A-dependent metabolism. J.Pharmacol. Exp. Ther. 1997;283:1552–62.
[32] Brzezinski MR, Boutelet-Bochan H, Person RE, Fantel AG, Juchau MR. Catalytic activity and quantitation of cytochrome P-450 2E1 in prenatal human brain. J.Pharmacol. Exp. Ther. 1999;289:1648–53.
[33] Thummel KE, Lee CA, Kunze KL, Nelson SD, Slattery JT. Oxidation of acetaminophen to N-acetyl-p-aminobenzoquinone imine by human CYP3A4. Biochem.-Pharmacol. 1993;45:1563–9.
[34] Kamiie J, Ohtsuki S, Iwase R, Ohmine K, Katsukura Y, Yanai K, et al. Quantitative atlas of membrane transporter proteins: development and application of a highly sensitive simultaneous LC/MS/MS method combined with novel in-silico peptide selection criteria. Pharm.Res. 2008;25:1469–83.
[35] Prasad B, Evers R, Gupta A, Hop CE, Salphati L, Shukla S, et al. Interindividual variability in hepatic organic anion-transporting polypeptides and P-glycoprotein (ABCB1) protein expression: quantification by liquid chromatography tandem mass spectroscopy and influence of genotype, age, and sex. Drug Metab.Dispos. 2014;42:78–88.
[36] Edson KZ, Prasad B, Unadkat JD, Suhara Y, Okano T, Guengerich FP, et al. Cytochrome P450-dependent catabolism of vitamin K: omega-hydroxylation catalyzed by human CYP4F2 and CYP4F11. Biochemistry 2013;52:8276–85.
[37] Shuster DL, Risler LJ, Liang CK, Rice KM, Shen DD, Hebert MF, et al. Maternal-fetal disposition of glyburide in pregnant mice is dependent on gestational age. J.Pharmacol. Exp. Ther. 2014;350:425–34.
[38] Nath A, Atkins WM. A theoretical validation of the substrate depletion approach to determining kinetic parameters. Drug Metab.Dispos. 2006;34:1433–5.
[39] Ravindran S, Basu S, Gorti SK, Surve P, Sloka N. Metabolic profile of glyburide in human liver microsomes using LC-DAD-Q-TRAP-MS/MS. Biomed.Chromatogr. 2013;27:575–82.
[40] Lee SJ, Goldstein JA. Functionally defective or altered CYP3A4 and CYP3A5 single nucleotide polymorphisms and their detection with genotyping tests. Pharmacogenomics 2005;6:357–71.
[41] Michaels S, Wang MZ. The revised human liver cytochrome P450 pie: absolute protein quantification of CYP4F and CYP3A enzymes using targeted quantitative proteomics. Drug Metab.Dispos. 2014;42:1241–51.
[42] Wang H, Xu D, Peng RX, Yue J. Testosterone-metabolizing capacity and characteristics of adrenal microsomes in human fetus in vitro. J.Pediatr. Endocrinol. Metab. 2010;23:143–52.
[43] Wang H, Ping J, Peng RX, Yue J, Xia XY, Li QX, et al. Changes of multiple biotransformation phase I and phase II enzyme activities in human fetal adrenals during fetal development. Acta Pharmacol. Sin. 2008;29:231–8.